ARCHIVES
of
FOUNDRY ENGINEERING

ISSN (2299-2944)
Volume 2025
Issue 4/2025

198 – 210

10.24425/afe.2025.157618

25/4

Published quarterly as the organ of the Foundry Commission of the Polish Academy of Sciences

Effects of Chromium Cast Iron Inoculations Made with Ferroalloys: FeNb vs FeTi

J. Mędoń [a, b, *], K.Z. Bracka-Kęsek [a], T. Wiktor [a], A. Świątkowski [a], M. Czarny [b], D. Kopyciński [a]

[a] AGH University of Krakow, al. Adama Mickiewicza 30, 30-059 Kraków, Poland
[b] Odlewnia „Świdnica" Sp. z o.o., Świdnica ul. Kliczkowska 53, 58-105 Świdnica, Poland
* Corresponding author: E-mail address: jasiek.medon@vp.pl

Received 06.06.2025; accepted in revised form 27.07.2025; available online 31.12.2025

Abstract

The subject of the work is to prove that correct inoculation improves the properties of high chromium cast iron. The analysis was performed in terms of the effect of Fe-Nb-based and Fe-Ti-based inoculators on the starting alloy. Defects in castings such as porosity cracks and shrinkage cavities are a huge problem for companies producing chromium iron range. Reducing the occurrence of the aforementioned defects will result in more profitable and repeatable production. A stabilized and controlled production process provides guarantees of competitiveness in terms of price as well as timing in the market. It seems that the procedure of inoculation of HCCI cast iron, which has not yet been implemented on an industrial scale, turns out to be helpful in these problems. The inoculation used should have a significant effect on the fragmentation of the primary austenite structure as well as affect the alloy in the area of carbide eutectic crystallization. The thesis that can be formulated is that the inoculation will allow to improve the functional properties of castings free from defects such as hot cracking. Industrial tests were carried out at the "Swidnica" Foundry Ltd. which made it possible to show that it is possible to perform correct inoculation of high chromium cast iron under the conditions of the foundry's production line. In addition, it was shown that the inoculation of Fe-Nb better than Fe-Ti affects the functional properties of the inoculated alloy. It turned out that a small addition of Fe-Ti inoculant leads to the formation of TiC carbides. In contrast, the formation of NbC carbide was not demonstrated in the study with the use of Fe-Nb inoculant. In this case, the formation of an intermetallic phase was observed.

Keywords: Inoculation, Inoculation in industry, High chromium cast iron, Minimizing casting cracking

1. Introduction

Swidnica Foundry Ltd. is a company that manufactures components for industries where high resistance to abrasive wear is required. Various industries require solutions that increase the life of operating components exposed to aggressive and highly abrasive factors. Production processes in the mining as well as energy industries are exposed to extreme abrasive as well as impact conditions. Materials that are used in these industries must be characterized by high abrasion resistance and crack resistance. Improving these properties in the material used for castings mounted in equipment will guarantee a reduction in operating costs as well as reduce downtime, resulting in improved production efficiency. Considering, for example, the cement industry, the improvement of abrasion and impact strength results in the possibility of increasing the throughput of the ground charge [1-6].

These alloys belong to the group of white cast irons, which are distinguished primarily by: a white-colored breakthrough and a structure in which graphite is absent, carbon is present in the metal matrix or bound in the form of carbides [7-10]. The high chromium content of high chromium cast iron allows it to achieve very good hardenability during heat treatment processes. Thanks

to the carbides present, it has very good resistance to abrasive wear, and thanks to the addition of chromium in its composition, it provides corrosion resistance. High-chromium cast iron has an important advantage all the parameters mentioned above retain their values at elevated temperatures, which is often very important when selecting structural materials in industries requiring wear resistance[11-16].

Chromium is the most common element chosen as an additive to increase hardness and the proportion of carbide precipitates. It is important that in the presence of other highly carbide-forming elements and a constant C content, chromium should be kept at a low level so as to protect against the formation of other hard carbides. The carbon content should be controlled so as to allow the formation of an adequate amount of other chromium carbides [17-19]. An increase in Cr content changes the structure and properties of chromium carbides from M_3C to M_7C_3 or $M_{23}C_6$ carbides. The symbol "M" denotes the elements that can be bound in the carbides, in the case of high chromium cast iron mainly Cr [20-22]. Of all carbides, M_7C_3 has the highest hardness which results in the least amount of wear loss [20]. Not all carbides develop a similar morphology. M_7C_3 carbide forms as isolated carbides as in the case of primary carbides, they form continuous crystal lattices between growing dendrites just like eutectic carbides [23-24]. Carbides whose interconnections are arranged in rods or plates are M3C and $M_{23}C_6$ carbides [24-26]. Table 1 presents the hardnesses of exemplary carbides.

Table 1.
Hardnesses of examples of carbides found in high chromium cast iron [27]

Carbide	Hardness (HV)
Boron carbide, B_4C	**1800 – 3500**
Titanium carbide, TiC	**2000 – 3200**
Vanadium carbide, VC	**2460 – 3150**
Niobium carbide, NbC	**2400 – 2850**
Tungsten carbide, WC	**2000 – 2400**
Chrome carbide type, M_7C_3	**1200 – 1800**
Chromium carbide type, $M_{23}C_6$	**1140 – 1500**
Molybdenum carbide, Mo_2C	**1500**
Chromium carbide type, M_3C	**1300**

An analysis of the literature on improving the wear resistance of Fe-C alloys indicates that, in addition to research conducted on classic wear-resistant alloys, such as high chromium cast irons, studies are often conducted on castings with wear-resistant composite zones [28-35] or in which the matrix throughout the volume is reinforced with carbides. The latter, which is realized during the metallurgical process, allows the entire volume of the liquid steel to produce primary carbides of vanadium, titanium or niobium either in a matrix of high-manganese austenite, Cr-Ni corrosion-resistant austenite or in alloyed martensitic and martensitic steel with residual austenite. In such alloys, during sand abrasion resistance tests, the authors obtained at least twice the abrasive wear resistance compared to reference samples. In these studies, the authors additionally point to the implicytny of the solution, the possibility of inoculating the liquid steel before casting, and the possibility of reducing the cost of smelting high-chromium alloys by partially replacing chromium with elements with a higher affinity for carbon [36-45].

Carbides with a wall-centered MC crystal structure are hard compounds introduced into HCCI cast iron to improve its wear resistance. A distinction is made between Zr, V, W, Ti, and Nb carbides [46-48]. Research in white cast iron has focused on vanadium, titanium, and niobium carbides [49-50].

NbC appears to be a very promising carbide resulting in improved properties of white cast iron due to its increased hardness. In his article, Guesser [51] described a study in which he added niobium to chromium cast iron with Cr content of 18%, and carbon content of 3%. He showed, niobium additions above 1% showed no significant improvement in the properties of these.

In order to improve the microstructure, it is necessary to change the carbide morphology, which improves the mechanical properties. The addition of inoculants during pouring such as TiC and NbC results in the introduction of heterogeneous M_7C_3 carbide nucleation pads into the alloy, resulting in improved microstructure of the casting. The addition of powdered niobium or titanium which reacted with carbon to form carbides in the matrix has been described in studies [52-55].

Production of high chromium iron castings, however, is associated with the occurrence of casting defects such as hot porosity cracks or shrinkage cavities. Example images of defects are shown in Figure 1.

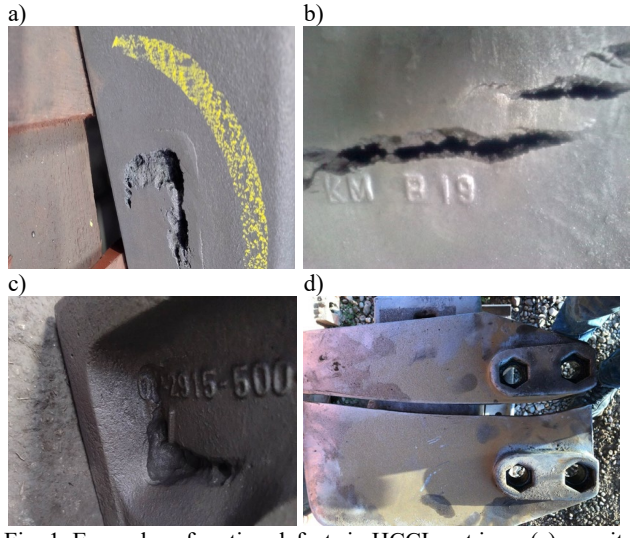

Fig. 1. Examples of casting defects in HCCI cast iron: (a)porosity, (b) hot cracking, (c) shrinkage cavity, (d) impact fracture

2. Phase analysis of cast iron performed with Thermocalc software

Diagrams from the ThermoCalc program showing curves of the molar proportion of each phase as a function of temperature are presented in the graphs. Figures 3 and 4 present the niobium-inoculation alloy with respect to the starting alloy for inoculation

(in Figure 2). Figures 5 and 6 present the titanium- inoculation alloy also in relation to the starting alloy for inoculation. From the phase diagrams showing changes in the occurrence and content of the various phases in the niobium- inoculation and titanium-inoculation high chromium cast iron, we can see several key changes depending on the increasing content of the inoculation element of the base alloy.

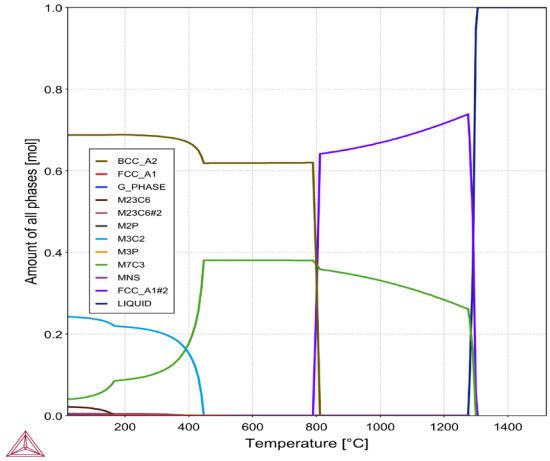

Fig. 2.. Molar contribution of individual phases as a function of temperature during solidification

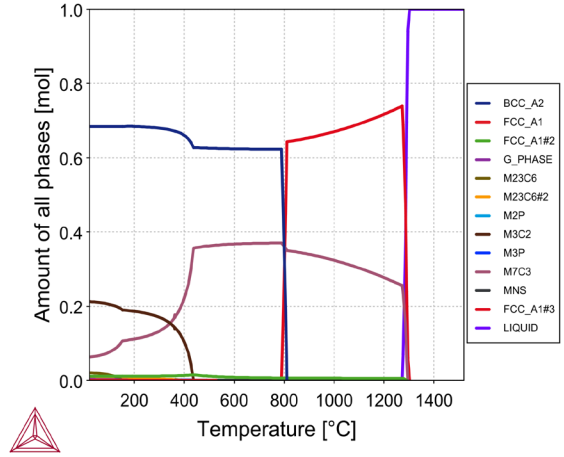

Fig. 3. Molar contribution of individual phases as a function of temperature during solidification- alloy inoculation 0,5% Nb

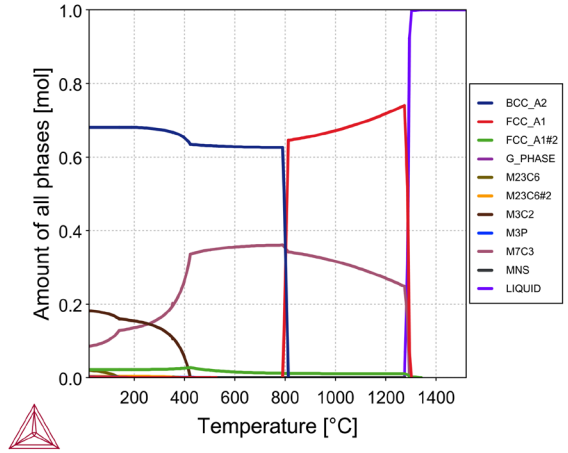

Fig.4. Molar contribution of individual phases as a function of temperature during solidification- alloy inoculation 1.0 % Nb

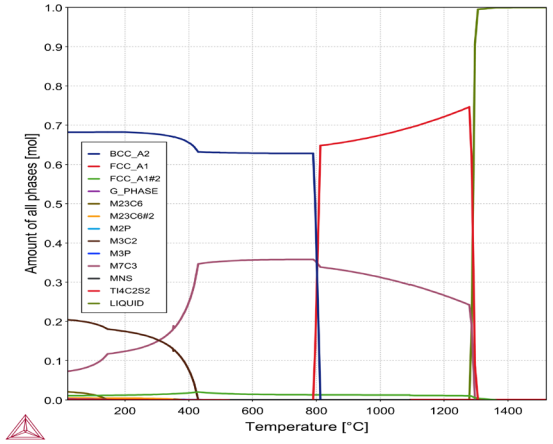

Fihg. 5. Molar contribution of individual phases as a function of temperature during solidification- alloy inoculation 0,5 % Ti

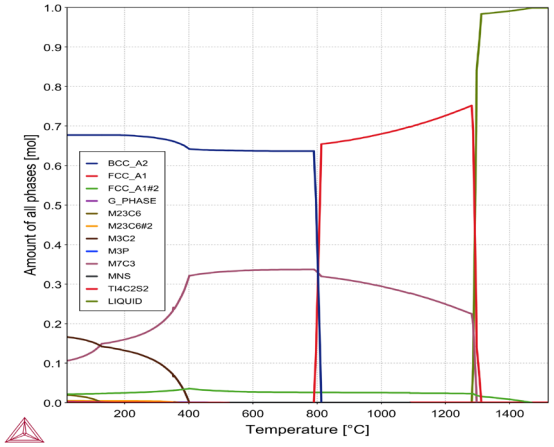

Fig. 6. Molar contribution of individual phases as a function of temperature during solidification- alloy inoculation 1.0% Ti

For each of the above diagrams, the mass fractions of each element in each of the phases present are summarized in Tables 2-6. Fe-Nb and Fe-Ti inoculation alloys are juxtaposed with the starting alloy for inoculation.

Table 2.
Phase composition of base alloy for inoculation

Phase	Fe	Si	Mn	Ni	Cr	P	Cu	Mo	C	S	Nb	Ti
Component	0,76	9,1E-03	7,8E-03	1,7E-03	0,20	2,5E-04	6,8E-04	8,9E-04	0,03	1,2E-04	0	0
BCC_A2#1	0,99	0,01	5,5E-05	3,9E-05	1,4E-06	1,5E-07	1,3E-09	6,3E-12	6,5E-13	5,8E-13	0	0
FCC_A1#1	3,4E-11	4,4E-13	1,2E-03	1,2E-05	8,2E-13	3,4E-11	0,9987	6,0E-09	1,9E-13	5,0E-13	0	0
G_PHASE#1	2,1E-12	0,13	0,22	0,64	0	0	0	0	0	0	0	0
M23C6#1	0,010	0	0,35	2,1E-07	0,59	0	0	1,3E-08	0,06	0	0	0
M23C6#2	0,17	0	5,2E-05	2,1E-06	0,57	0	0	0,20	0,05	0	0	0
M2P#1	0,04	0	0	0,75	6,7E-04	0,21	0	0	0	0	0	0
M3C2#1	0	0	0	0,00	0,87	0	0	7,4E-12	0,13	0	0	0
M3P#1	0,52	0	0	0,13	0,20	0,16	9,7E-13	0	0	0	0	0
M7C3#1	6,3E-04	4,9E-13	0,01	2,4E-10	0,90	0	0	2,4E-06	0,09	0	0	0
MNS#1	6,4E-13	0	0,63	0	0	0	7,3E-13	0	0	0,37	0	0

Table 3.
Phase composition of the inoculation alloy 0,5% Nb

Phase	Fe	Si	Mn	Ni	Cr	P	Cu	Mo	C	S	Nb	Ti
Component	0,75	9,1E-03	7,8E-03	1,7E-03	0,20	2,5E-04	6,5E-04	8,9E-04	0,03	1,2E-04	5,0E-03	0
BCC_A2#1	0,99	0,01	5,5E-05	3,9E-05	1,4E-06	1,5E-07	1,3E-09	6,3E-12	6,5E-13	5,8E-13	1,7E-12	0
FCC_A1#1	3,4E-11	4,4E-13	1,2E-03	1,2E-05	8,2E-13	3,4E-11	1E+00	6,0E-09	1,9E-13	5,0E-13	1,5E-12	0
FCC_A1#2	2,8E-09	3,3E-13	1,9E-06	6,0E-10	0,32	3,7E-13	7,6E-13	1,1E-12	0,14	3,8E-13	0,54	0
G_PHASE#1	2,0E-12	0,13	0,22	0,64	0	0	0	0	0	0	4,8E-04	0
M23C6#1	9,8E-03	0	0,35	2,1E-07	0,59	0	0	1,3E-08	0,06	0	0	0
M23C6#2	0,17	0	5,2E-05	2,1E-06	0,57	0	0	0,20	0,05	0	0	0
M2P#1	0,04	0	0	0,75	6,7E-04	0,21	0	0	0	0	0	0
M3C2#1	0	0	0	0	0,87	0	0	7,4E-12	0,13	0	0	0
M3P#1	0,52	0	0	0,13	0,20	0,16	9,7E-13	0	0	0	0	0
M7C3#1	6,3E-04	4,9E-13	0,01	2,4E-10	0,90	0	0	2,4E-06	9,0E-02	0	1,6E-12	0
MNS#1	6,4E-13	0	0,63	0	0	0	7,3E-13	0	0	0,37	0	0

Table 4.
Phase composition of the inoculation alloy 1.0 % Nb

Phase	Fe	Si	Mn	Ni	Cr	P	Cu	Mo	C	S	Nb	Ti
Component	0,75	9,1E-03	7,8E-03	1,8E-03	0,195	2,5E-04	6,4E-04	8,9E-04	0,03	1,2E-04	0,01	0
BCC_A2#1	9,9E-01	0,01	5,5E-05	3,9E-05	1,4E-06	1,5E-07	1,3E-09	6,3E-12	6,5E-13	5,8E-13	1,7E-12	0
FCC_A1#1	3,4E-11	4,4E-13	1,3E-03	1,2E-05	8,2E-13	3,4E-11	1E+00	6,0E-09	1,9E-13	5,0E-13	1,5E-12	0
FCC_A1#2	2,8E-09	3,3E-13	1,9E-06	6,0E-10	0,32	3,7E-13	7,6E-13	1,1E-12	0,14	3,8E-13	0,54	0
G_PHASE#1	2,0E-12	0,13	0,22	0,64	0	0	0	0	0	0	4,8E-04	0
M23C6#1	9,8E-03	0	0,35	2,1E-07	0,59	0	0	1,3E-08	0,06	0	0	0
M23C6#2	0,17	0	5,2E-05	2,1E-06	0,57	0	0	0,20	0,05	0	0	0
M3C2#1	0	0	0	0	0,87	0	0	7,4E-12	0,13	0	0	0
M3P#1	0,52	0	0	0,13	0,20	0,16	9,7E-13	0	0	0	0	0
M7C3#1	6,3E-04	4,9E-13	1,1E-02	2,3E-10	0,90	0	0	2,4E-06	0,09	0	1,6E-12	0
MNS#1	6,4E-13	0	0,63	0	0	0	7,3E-13	0	0	0,37	0	0

Table 5.
Phase composition of the inoculation alloy 0,5% Ti

Phase	Fe	Si	Mn	Ni	Cr	P	Cu	Mo	C	S	Ti	Nb
Component	0,75	0,01	7,8E-03	1,8E-03	0,20	2,5E-04	6,5E-04	8,9E-04	0,03	1,2E-04	0,01	0
BCC_A2#1	9,9E-01	0,01	5,5E-05	3,9E-05	1,4E-06	1,5E-07	1,3E-09	6,3E-12	6,5E-13	5,8E-13	8,7E-13	0
FCC_A1#1	3,4E-11	4,4E-13	1,3E-03	1,2E-05	8,2E-13	3,4E-11	1E+00	6,0E-09	1,9E-13	5,0E-13	7,5E-13	0
FCC_A1#2	9,3E-13	4,7E-13	2,7E-06	9,8E-13	3,0E-02	5,2E-13	1,1E-12	3,4E-10	0,20	5,3E-13	0,77	0
G_PHASE#1	2,1E-12	1,3E-01	0,22	0,64	0	0	0	0	0	0	7,4E-10	0
M23C6#1	0,01	0	0,35	2,1E-07	0,59	0	0	1,3E-08	0,06	0	0	0
M23C6#2	0,17	0	5,2E-05	2,1E-06	0,57	0	0	0,20	0,05	0	0	0
M2P#1	0,04	0	0	0,75	6,8E-04	0,21	0	0	0	0	0	0
M3C2#1	0	0	0	0	0,87	0	0	7,4E-12	0,13	0	0	0
M3P#1	0,52	0	0	0,13	0,20	0,16	9,7E-13	0	0	0	0	0
M7C3#1	6,3E-04	4,9E-13	0,01	2,4E-10	0,90	0	0	2,4E-06	0,09	0	0	0
MNS#1	6,4E-13	0	0,63	0	0	0	7,3E-13	0	0	0,37	0	0
TI4C2S2#1	0	0	0	0	0	0	0	0	8,6E-02	2,3E-01	6,8E-01	0

Table 6.
Phase composition of the inoculation alloy 1.0% Ti

Phase	Fe	Si	Mn	Ni	Cr	P	Cu	Mo	C	S	Ti	Nb
Component	0,75	0,01	0,01	1,7E-03	0,20	2,5E-04	6,5E-04	8,9E-04	2,8E-02	1,3E-04	0,01	0
BCC_A2#1	0,99	0,01	5,5E-05	3,9E-05	1,4E-06	1,5E-07	1,3E-09	6,3E-12	6,5E-13	5,8E-13	8,7E-13	0
FCC_A1#1	3,4E-11	4,4E-13	1,2E-03	1,2E-05	8,2E-13	3,4E-11	1E+00	6,0E-09	1,9E-13	5,0E-13	7,5E-13	0
FCC_A1#2	9,3E-13	4,7E-13	2,7E-06	9,8E-13	0,03	5,2E-13	1,1E-12	3,4E-10	2,0E-01	5,3E-13	7,7E-01	0
G_PHASE#	2,1E-12	0,13	0,22	0,64	0	0	0	0	0	0	7,4E-10	0
M23C6#1	0,01	0	0,35	2,1E-07	0,59	0	0	1,3E-08	5,6E-02	0	0	0
M23C6#2	0,17	0	5,2E-05	2,1E-06	0,57	0	0	0,20	5,1E-02	0	0	0
M3C2#1	0	0	0	0	0,87	0	0	7,4E-12	1,3E-01	0	0	0
M3P#1	0,52	0	0	0,13	0,20	0,16	9,7E-13	0	0	0	0	0
M7C3#1	6,3E-04	4,9E-13	0,01	2,3E-10	0,90	0	0	2,4E-06	9,0E-02	0	0	0
MNS#1	6,4E-13	0	0,63	0	0	0	7,3E-13	0	0	3,7E-01	0	0
TI4C2S2#1	0	0	0	0	0	0	0	0	8,6E-02	2,3E-01	6,8E-01	0

3. Research Methodology

The melting was carried out in a 2-ton medium-frequency induction furnace from Termetal. The metal was poured into an intermediate ladle (1500°C), in which transport to the pouring station was realized. The inoculator was dosed onto the metal stream during pouring. The dosing temperature of the inoculator with a granulation of 0.2 0.7mm was 1420°C. The inoculators used in the study were Fe-Nb and Fe-Ti. The chemical composition is presented in Table 7.

Table 7.
Chemical composition of individual alloys

	Element [% mas.]										
	C	Si	Mn	P	S	Cr	Ni	Cu	Ti	Nb	Al.
Reference I	2,93	0,645	0,855	0,0205	0,0252	20,66	0,181	0,055	0,0014	<0,001	0,0022
0,15 % FeNb	2,92	0,644	0,850	0,0223	0,0252	20,66	0,182	0,055	0,0015	0,088	0,0023
0,31 % FeNb	2,93	0,648	0,852	0,0223	0,0253	20,60	0,180	0,054	0,0011	0,179	0,0020
0,77 % FeNb	2,90	0,646	0,854	0,0224	0,0252	20,62	0,182	0,056	0,0013	0,495	0,0025
1,08 % FeNb	2,90	0,647	0,854	0,0223	0,0251	20,66	0,183	0,055	0,0015	0,710	0,0022
1,54 % FeNb	2,89	0,645	0,856	0,0223	0,0251	20,65	0,181	0,056	0,0017	0,952	0,0022
2,31 % FeNb	2,90	0,648	0,856	0,0224	0,0252	20,65	0,182	0,056	0,0015	1,489	0,0021
Reference II	2,94	0,645	0,853	0,0215	0,0262	20,66	0,382	0,055	0,0014	<0,001	0,0024
0,13 % FeTi	2,92	0,644	0,854	0,0206	0,0253	20,66	0,183	0,054	0,0551	<0,001	0,0025
0,27 % FeTi	2,90	0,645	0,856	0,0205	0,0252	20,65	0,182	0,055	0,0978	<0,001	0,0023
0,67 % FeTi	2,90	0,645	0,855	0,0205	0,0253	20,66	0,182	0,054	0,352	<0,001	0,0026
0,93 % FeTi	2,89	0,644	0,855	0,0206	0,0252	20,64	0,183	0,056	0,601	<0,001	0,0025
1,33 % FeTi	2,89	0,646	0,856	0,0204	0,0253	20,66	0,181	0,056	0,925	<0,001	0,0024
2,00 % FeTi	2,88	0,645	0,854	0,0203	0,0253	20,65	0,182	0,056	1,442	<0,001	0,0024

3.1. Metallographic Analysis

The samples for metallographic analysis were made with a Struers Tegramin - 20 laboratory grinding and polishing machine using magnetic abrasive discs with gradations from 120 to 1200, using water as a cooling and lubricating medium. During grinding, the speed of the disc was 300rpm, and the samples were pressed against the disc with a force of 40N. The samples were then polished on MD - NAP polishing cloth in the presence of DP - Lubricant Blue and 9µm and 3µm diamond slurry. The samples were polished at a disc speed of 150rpm and a pressure of up to 25N. The metallographic specimens prepared in this way were

etched with Vilell'a reagent for approximately one minute - to obtain adequate contrast between the phases present.

Microstructure images were taken on a MEF - 4M by Leica. Optical microscopy was used to determine the fragmentation of the microstructure along with an analysis.

On the other hand, SEM technology was used to determine the morphology of the precipitates present in the microstructure and to study the chemical composition of the different phases using an EDS detector.

3.2. Tests of resistance to hot cracking - Althoff-Radtke test

As part of the work, a study was carried out on the resistance of cast iron to hot cracking. A base alloy melting was performed and a inoculation procedure was carried out with ferroalloys: Fe-Nb and Fe-Ti. Each inoculation alloy was poured into a mold, which contained a model of the A-R test. An example of the mold is presented in Figure 7.

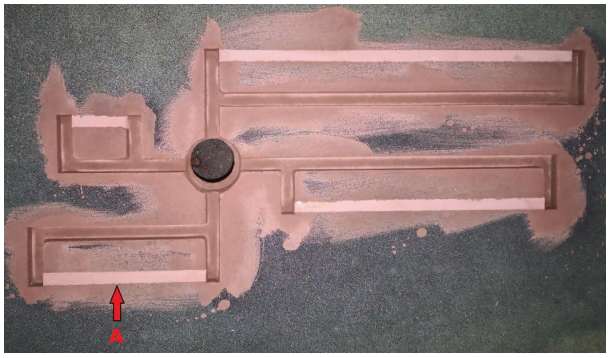

Fig. 7. Form with strut rods installed (A)

Breaks were taken from the longest of the brackets at the corners, where the risk of hot cracking is greatest. This step of the study focused on comparing the breakthroughs obtained in tests with the addition of different amounts of inoculator relative to the base alloy for inoculation. The breakthrough results of the Althoff-Radtke method are shown in Figures 8 and 9. In each photograph, from left: the base alloy, and inoculation with a particular dose of the inoculation element, which was Nb in the first case, and Ti in the second case.

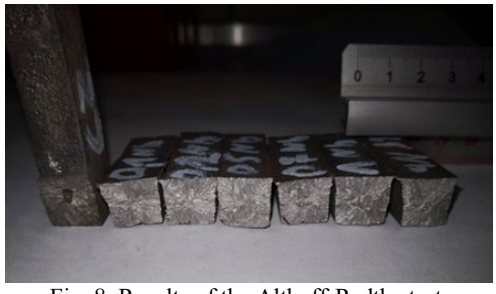

Fig. 8. Results of the Althoff-Radtke test:
From left, reference sample; 0.15 % Fe-Nb; 0.31 % Fe-Nb; 0.77 % Fe-Nb; 1.08 % Fe-Nb; 1.54 % Fe-Nb; 2.31 %Fe-Nb.

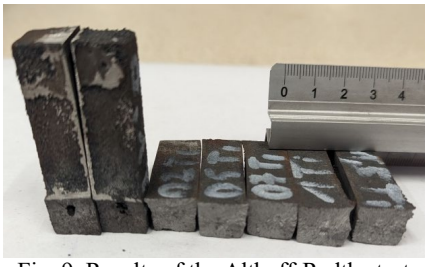

Fig. 9. Results of the Althoff-Radtke test
From left, reference sample; 0.13 % Fe-Ti; 0.27 % Fe-Ti; 0.67 % Fe-Ti; 0.93 % Fe-Ti; 1.33 % Fe-Ti; 2.00 % Fe-Ti.

In the absence of buckle breakage during solidification, mechanical breakage of unbroken buckles was necessary. The conducted tests made it possible to check which inoculating element has the best effect on eliminating hot cracking. The element with the greatest inoculating potential turned out to be niobium. No cracking occurred on any of the buckles; all of the buckles had to be mechanically fixed. The longest of the buckles had a small crack but without black areas, which indicates that there was no hot cracking but cold cracking, which probably occurred when the casting was pulled from the mold. The 50mm, 150mm and 250mm buckles showed no cracks, so only the breakthroughs taken from the longest buckles, where the risk of hot cracking is greatest, are summarized in Figures 8 and 9.

The use of titanium as a inoculation element also reduced the occurrence of hot cracking relative to the starting sample for the inoculation treatment. In Figure 9, it can be observed that at 0.13% Ti content there was a black area, which indicates that hot cracking occurred but only on the longest of the buckles. The breaks of buckles of lengths 50, 150, 250mm did not show hot cracking. The dosage of higher titanium content surfaced to eliminate the occurrence of hot cracking of the inoculation alloys. **The titanium and niobium contents of the liquid alloy were chosen for further study at 0.5% and 0.7%.**

3.3. Casting of specimens intended for strength properties testing

In the following experiments, two melt inoculation were carried out: 0.67%, 0.93 Fe-Ti and 0.77% and 1.08% Fe-Nb. The chemical compositions of the melts are shown in Table 8. The inoculator was dosed into the metal boil at 1460ºC From these melts, samples were prepared for strength tests..

Table 8.
Chemical composition of smelts sampled for strength and abrasion testing

	Element [% mas.]										
	C	Si	Mn	P	S	Cr	Ni	Cu	Ti	Nb	Al.
Reference I	2.93	0.645	0.855	0.0205	0.0252	20.66	0.181	0.055	0.0014	<0.001	0.0022
0.77 % FeNb	2.90	0.646	0.854	0.0224	0.0252	20.62	0.182	0.056	0.0013	0.495	0.0025
1.08 % FeNb	2.90	0.647	0.854	0.0223	0.0251	20.66	0.183	0.055	0.0015	0.710	0.0022
Reference II	2.94	0.645	0.853	0.0215	0.0262	20.66	0.182	0.055	0.0014	<0.001	0.0024
0.67 % FeTi	2.90	0.645	0.855	0.0205	0.0253	20.66	0.182	0.054	0.352	<0.001	0.0026
0.93 % FeTi	2.89	0.644	0.855	0.0206	0.0252	20.64	0.183	0.056	0.601	<0.001	0.0025

3.4. Impact resistance and hardness

A Charpy pendulum hammer 300J was used for the tests. The test involves breaking a sample placed in the lower part of the hammer. The arm, moving under the influence of gravity, strikes the sample and breaks it. The hammer is equipped with a scale on which we can directly read the energy used to break the sample or the maximum angle of deflection.

Hardness was tested using the Rockwell method. The test consisted of measuring the increase in the depth of the indentation. A diamond cone with an angle of 120° and a tip radius of 0.2 mm was used as the indenter. Due to the hardness of the tested material, the HRC scale was used for the tests. The measurement consisted of pressing the cone into the tested material in two stages at right angles. After releasing the force, the result on the C scale was read on a microscope on the device.

4. Research results

4.1. Optical microscope structure of starting cast iron for inoculation

Microstructures of chrome cast iron starting for inoculation made on optical microscope are shown in Figure 10.

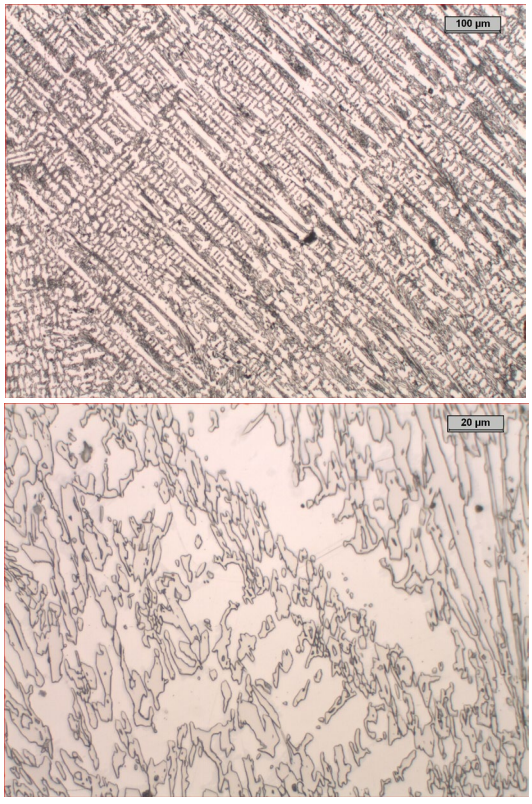

a)

b)

Fig. 10. Microstructure of starting cast iron for inoculation: (a) 100x magnification, (b) 500x magnification

4.2. SEM analysis of Fe-Nb- inoculated cast iron

Figures 11 and 12 show SEM microstructure imaging. The EDS detector images were taken at 1000x magnification to accurately measure the chemical composition for each phase. The analysis showed the existence of chromium carbides in the structure of the primary phase and a chromium iron matrix characterized by a characterized by a high content of the alloying element Cr.

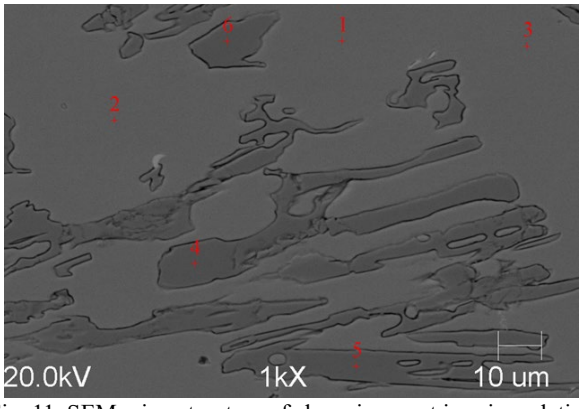

Fig. 11. SEM microstructure of chromium cast iron inoculation with 0.77% Fe-Nb, EDS chemical composition at the marked points is given below the figure

Point 2

Elt.	Line	Intensity (c/s)	Error 2-sig	Gauss Fit	Atomic %	Conc	
C	Ka	1.15	0.391	0.37	23.307	6.244	wt.%
Si	Ka	2.39	0.564	0.15	1.467	0.919	wt.%
P	Ka	0.65	0.294	0.78	0.328	0.227	wt.%
S	Ka	0.13	0.134	0.18	0.057	0.041	wt.%
Cr	Ka	27.77	1.924	0.91	8.661	10.045	wt.%
Mn	Ka	0.00	0.000	0.31	0.000	0.000	wt.%
Fe	Ka	120.06	4.001	2.64	66.076	82.309	wt.%
Nb	La	0.34	0.214	0.27	0.104	0.216	wt.%
					100.000	100.000	wt.%

Point 4

Elt.	Line	Intensity (c/s)	Error 2-sig	Gauss Fit	Atomic %	Conc	
C	Ka	3.50	0.683	0.97	43.571	14.802	wt.%
Si	Ka	1.10	0.384	0.23	0.465	0.370	wt.%
P	Ka	0.15	0.140	0.00	0.051	0.045	wt.%
S	Ka	0.26	0.187	0.18	0.078	0.071	wt.%
Cr	Ka	107.20	3.781	2.60	33.168	48.781	wt.%
Mn	Ka	2.21	0.543	0.56	0.752	1.169	wt.%
Fe	Ka	48.48	2.542	1.62	21.773	34.392	wt.%
Nb	La	0.70	0.306	0.28	0.141	0.370	wt.%
					100.000	100.000	wt.%

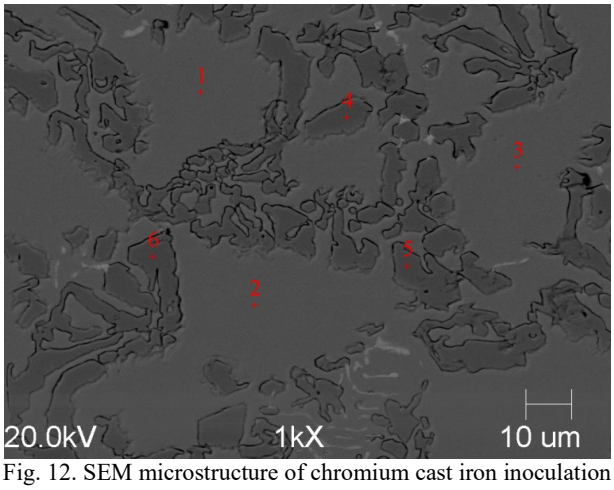

Fig. 12. SEM microstructure of chromium cast iron inoculation with 1.08%Fe-Nb, EDS chemical composition at the marked points is given below the figure

Point 3

Elt.	Line	Intensity (c/s)	Error 2-sig	Gauss Fit	Atomic %	Conc	
C	Ka	1.05	0.374	0.72	23.846	6.392	wt.%
Si	Ka	1.35	0.424	0.32	0.938	0.588	wt.%
P	Ka	0.21	0.168	0.22	0.121	0.084	wt.%
S	Ka	0.00	0.000	0.30	0.000	0.000	wt.%
Cr	Ka	25.84	1.856	0.94	9.204	10.680	wt.%
Mn	Ka	0.00	0.000	0.27	0.000	0.000	wt.%
Fe	Ka	105.26	3.746	2.01	65.731	81.922	wt.%
Nb	La	0.47	0.250	0.30	0.161	0.334	wt.%
					100.000	100.000	wt.%

Point 6

Elt.	Line	Intensity (c/s)	Error 2-sig	Gauss Fit	Atomic %	Conc	
C	Ka	2.64	0.593	0.60	40.515	13.285	wt.%
Si	Ka	0.84	0.335	0.28	0.435	0.334	wt.%
P	Ka	0.22	0.171	0.35	0.094	0.079	wt.%
S	Ka	0.18	0.153	0.27	0.064	0.056	wt.%
Cr	Ka	91.83	3.499	2.23	34.519	49.002	wt.%
Mn	Ka	1.35	0.424	0.51	0.556	0.834	wt.%
Fe	Ka	43.35	2.404	1.54	23.721	36.167	wt.%
Nb	La	0.39	0.229	0.13	0.096	0.243	wt.%
					100.000	100.000	wt.%

4.3. SEM analysis of Fe-Ti inoculated cast iron

Figures 13 and 14 show SEM microstructure imaging. The EDS detector images were taken at 1000x magnification to accurately measure the chemical composition for each phase. The analysis showed the existence of chromium carbides in the structure of the primary phase and a chromium iron matrix characterized by a characterized by a high content of the alloying element Cr.

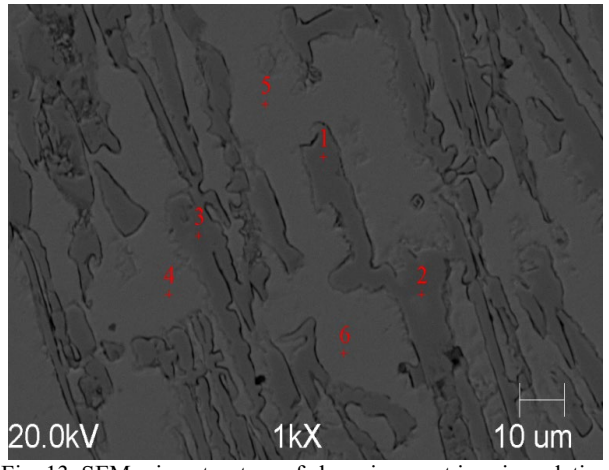

Fig. 13. SEM microstructure of chromium cast iron inoculation with 0.67%Fe-Ti, EDS chemical composition at the marked points is given below the figure

Point 1

Elt.	Line	Intensity (c/s)	Error 2-sig	Gauss Fit	Atomic %	Conc	
C	Ka	2.13	0.533	0.68	41.343	13.710	wt.%
Si	Ka	0.33	0.208	0.30	0.214	0.166	wt.%
P	Ka	0.32	0.205	0.27	0.172	0.147	wt.%
S	Ka	0.49	0.256	0.30	0.227	0.201	wt.%
Ti	Ka	0.00	0.000	0.00	0.000	0.000	wt.%
Cr	Ka	72.49	3.109	1.88	34.840	50.015	wt.%
Mn	Ka	1.04	0.373	0.47	0.551	0.836	wt.%
Fe	Ka	32.41	2.079	0.96	22.652	34.925	wt.%
					100.000	100.000	wt.%

Point 4

Elt.	Line	Intensity (c/s)	Error 2-sig	Gauss Fit	Atomic %	Conc	
C	Ka	0.49	0.255	0.47	15.433	3.843	wt.%
Si	Ka	1.37	0.427	0.32	1.311	0.764	wt.%
P	Ka	0.10	0.116	0.30	0.078	0.050	wt.%
S	Ka	0.30	0.202	0.27	0.199	0.132	wt.%
Ti	Ka	0.17	0.148	0.38	0.076	0.075	wt.%
Cr	Ka	21.80	1.705	1.23	10.595	11.421	wt.%
Mn	Ka	0.00	0.000	0.37	0.000	0.000	wt.%
Fe	Ka	85.13	3.369	2.05	72.307	83.714	wt.%
					100.000	100.000	wt.%

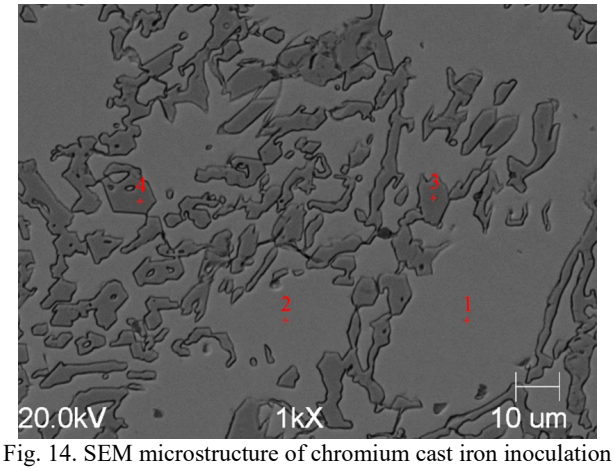

Fig. 14. SEM microstructure of chromium cast iron inoculation with 0.93% Fe-Ti, EDS chemical composition at the marked points is given below the figure

Point 2

Elt.	Line	Intensity (c/s)	Error 2-sig	Gauss Fit	Atomic %	Conc	
C	Ka	0.57	0.276	0.54	18.451	4.742	wt.%
Si	Ka	1.75	0.483	0.12	1.709	1.027	wt.%
P	Ka	0.42	0.236	0.21	0.336	0.223	wt.%
S	Ka	0.16	0.146	0.00	0.108	0.074	wt.%
Ti	Ka	0.23	0.173	0.27	0.108	0.111	wt.%
Cr	Ka	21.26	1.683	0.69	10.915	12.144	wt.%
Mn	Ka	1.80	0.490	0.21	0.993	1.167	wt.%
Fe	Ka	76.93	3.203	1.71	67.381	80.514	wt.%
					100.000	100.000	wt.%

Point 4

Elt.	Line	Intensity (c/s)	Error 2-sig	Gauss Fit	Atomic %	Conc	
C	Ka	1.89	0.502	0.34	39.394	12.774	wt.%
Si	Ka	0.33	0.211	0.32	0.237	0.180	wt.%
P	Ka	0.32	0.206	0.56	0.186	0.156	wt.%
S	Ka	0.12	0.129	0.30	0.062	0.054	wt.%
Ti	Ka	0.85	0.336	0.13	0.268	0.347	wt.%
Cr	Ka	69.61	3.046	1.93	35.949	50.465	wt.%
Mn	Ka	1.02	0.368	0.58	0.576	0.855	wt.%
Fe	Ka	31.07	2.035	1.18	23.327	35.170	wt.%
					100.000	100.000	wt.%

4.4. Identification of phases in Fe-Nb and Fe-Ti inoculated irons

Figures 15 and 16 present scanning microscope images from which the phase analysis was performed using EDS chemical composition. When an Nb-based inoculator is used, a niobium-rich intermetallic phase is formed in addition to carbides in the structure.

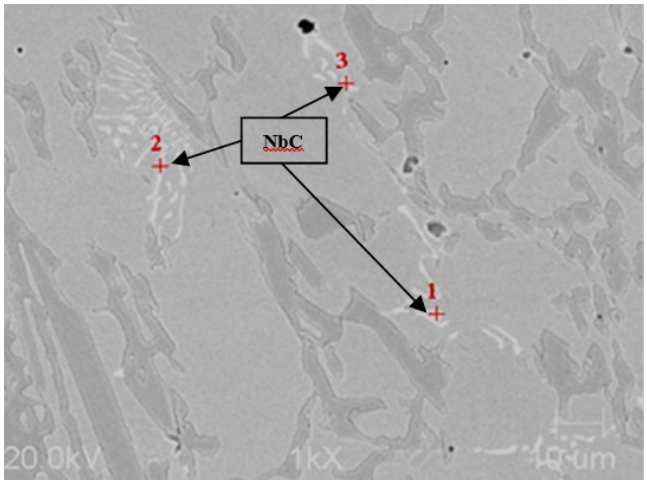

Fig. 15. SEM microstructure of Fe-Nb- inoculation chromium cast iron, EDS chemical composition spectra at labeled points are provided below the figure

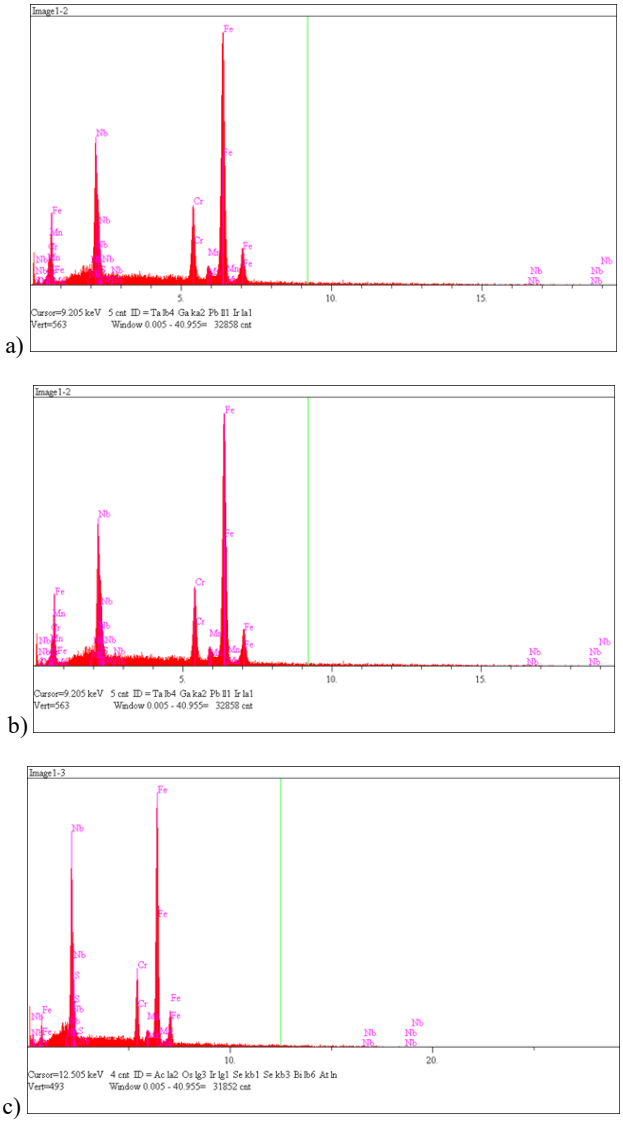

Fig. 16. EDS analysis spectra for the measurement points in Figure 15: (a) point 1; (b) point 2; (c) point 3

Using a titanium-based innoculator, carbides and sulfides are formed in the structure as shown in Figure 17. EDS spectra allowed assessment of the chemical composition at each point in the structure. figure 18. Figure 19 presents the microstructures of the reduced carbon melt. The images are shown for illustrative purposes to show the reduction of carbides present in the alloys.

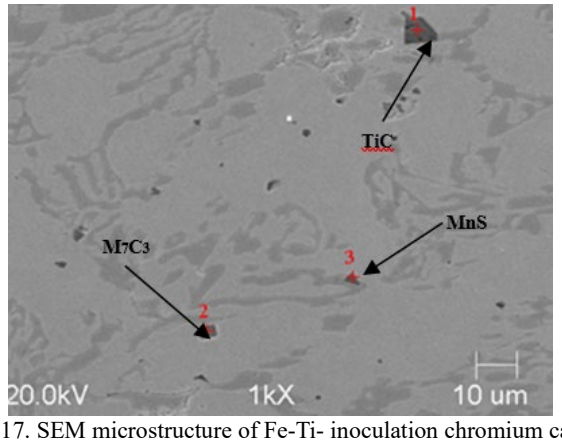

Fig. 17. SEM microstructure of Fe-Ti- inoculation chromium cast iron, EDS chemical composition spectra at labeled points are provided below the figure

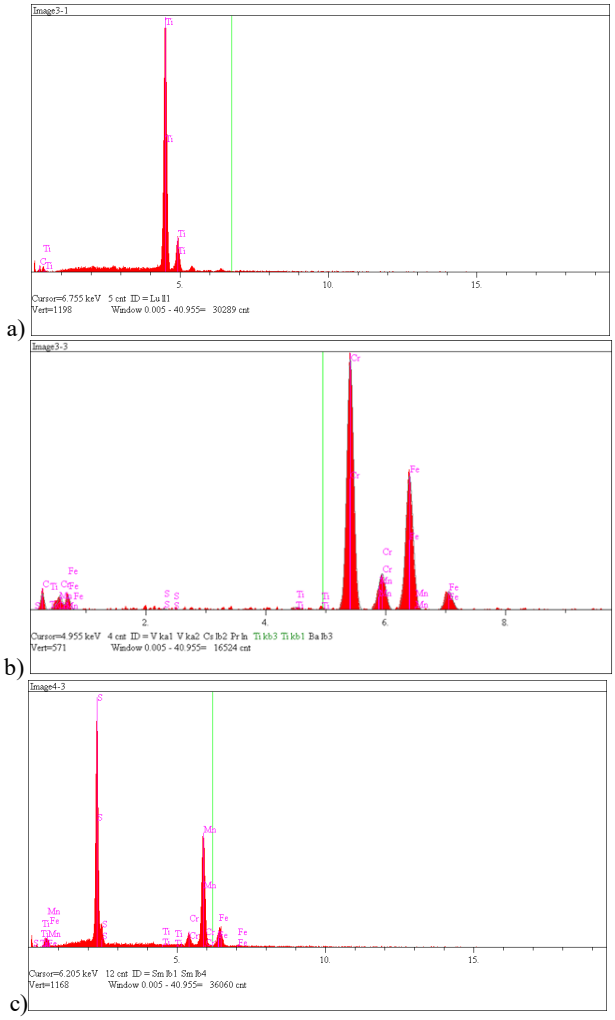

Fig. 18. EDS analysis spectra for the measurement points in Figure 17: (a) point 1; (b) point 2; (c) point 3

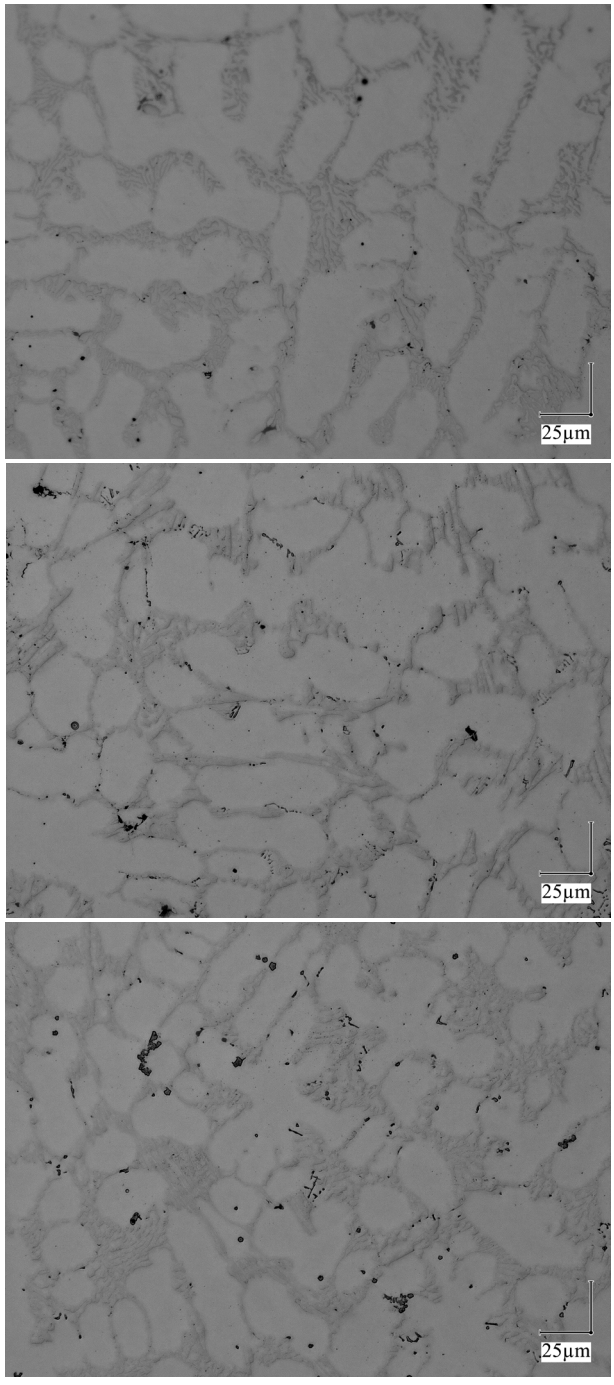

Fig.19. Microstructures of a reduced carbon melt: a) Reference II, b) inoculation Fe-Nb, c) inoculation Fe-Ti

4.5. Impact resistance and hardness

From the graph in figure 20, it is possible to analyse the properties of high-chromium cast iron inoculation with Fe-Ti and Fe-Nb additives in two melt variants - with a carbon content of

3% (first melt) and 2% (second melt). This figure shows the results of hardness and impact strength of the samples without tempered. The results of the samples tempered at 950º are shown in figure 21

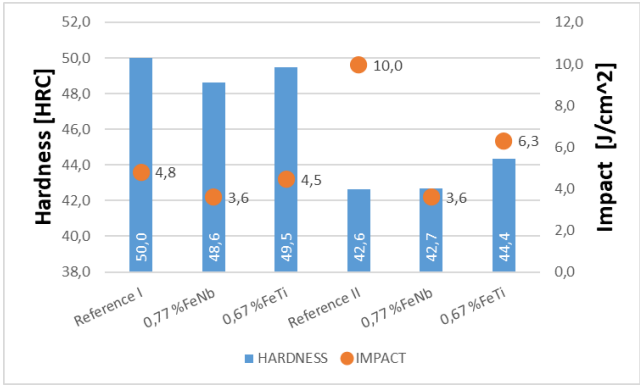

Fig.20. Impact strength and hardness - melting with higher inoculation injection temperature- without tempered

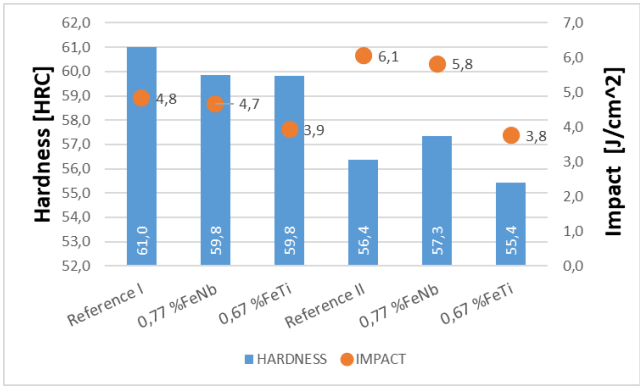

Fig. 21. Impact strength and hardness - melting with higher innoculation injection temperature- tempered 950º C

5. Summary of research

The conducted research on the impact of adding inoculators to the base alloy of high-chromium cast iron allowed us to assess which of the inoculants has a better effect on the properties of the base alloy.

Thanks to simulations carried out in the ThermoCalc program, it was possible to analyze the impact of individual inoculators on changes in the formation of individual phases. The evaluation of the molar fractions of individual phases showed in which phase the highest content of the element used during the inoculation process was found.

Based on the simulation results, smelting was carried out under industrial conditions at the "Swidnica" Foundry Ltd, during which Althoff-Radtke castings were poured, on the basis of which it was assessed how inoculation with individual inoculators affects the reduction of the tendency of high-chromium cast iron to crack. In this study, niobium proved to be a slightly better inoculator, thanks to which breaks without visible cracks formed during the solidification of the casting were obtained. In the case of inoculation with titanium in the amount of 0.13% Fe-Ti, a crack formed in the corner of the clamp.

Based on the analysis of the tests performed, the optimal content of individual inoculation was selected as 0.67% and 0.93% Fe-Ti and 0.77% and 1.08% Fe-Nb. Metallographic images under an optical microscope show how titanium and niobium affect changes in the microstructure. Thanks to the addition of inoculants to the initial alloy, which was characterized by the presence of large dendrites, the microstructure was fragmented and the homogeneity of carbide precipitates was increased. SEM analysis showed the chemical composition of the tested phase and which phase is richest in the elements used as inoculators.

An analysis of the graph showing the mechanical properties of raw cast iron samples (without hardening) revealed a significant impact of carbon content and inoculant type on hardness and impact strength. Reference sample I, containing approximately 3% C, achieved the highest hardness (50.0 HRC), but with low impact strength (4.8 J/cm²). Reducing the carbon content to 2% (reference sample II) resulted in a significant increase in impact strength (10.0 J/cm²), but at the expense of hardness (42.6 HRC). The addition of 0.77% Fe-Nb at a higher carbon content resulted in moderate hardness (48.6 HRC) and poorer impact strength (3.6 J/cm²). Fe-Ti (0.67%) at 3% C resulted in higher hardness (49.5 HRC) and impact strength of 4.5 J/cm², making it more effective than Fe-Nb. At lower carbon content, Fe-Nb did not bring any benefits – hardness dropped to 42.7 HRC and impact strength to only 3.6 J/cm². Fe-Ti at 2% C increased hardness to 44.4 HRC and provided moderate impact strength (6.3 J/cm²). The use of inoculators therefore has different effects on the alloy composition. Fe-Nb performs worse at higher carbon content, while Fe-Ti gives better results. The results confirm that without hardening, optimal performance is not achieved and heat treatment is necessary to fully exploit the potential of the inoculants.

Analysis of the hardness and impact strength results of samples hardened at 950°C from two alloys showed that the addition of Fe-Nb (0.77%) affects the hardness of cast iron (59.8 HRC in the first alloy and 57.3 HRC in the second alloy) with a slight decrease in impact strength. On the other hand, Fe-Ti (0.67%) causes a decrease in impact strength (to 3.9 and 3.8 J/cm²) with comparable or lower hardness, making it a less favourable inoculator. Reducing the carbon content in the second alloy increases impact strength but may lead to a slight decrease in hardness after inoculation. Fe-Nb maintains a better balance between hardness and impact strength than Fe-Ti.

Figure 22 shows a problematic casting that cracked during solidification under industrial conditions at the "Swidnica" Foundry Ltd. During melting, Fe-Nb inoculation was used, which made it possible to produce a crack-free casting. The Fe-Ti inoculant cannot be overlooked, as it also causes fragmentation of the structure to an extent that allows for the production of a crack-free casting. The complex design of the casting, which is characterized by high internal stresses, caused the casting to crack, if not during cooling, then during hardening. Inoculation of the alloy made it possible to eliminate this problem.

a) b)

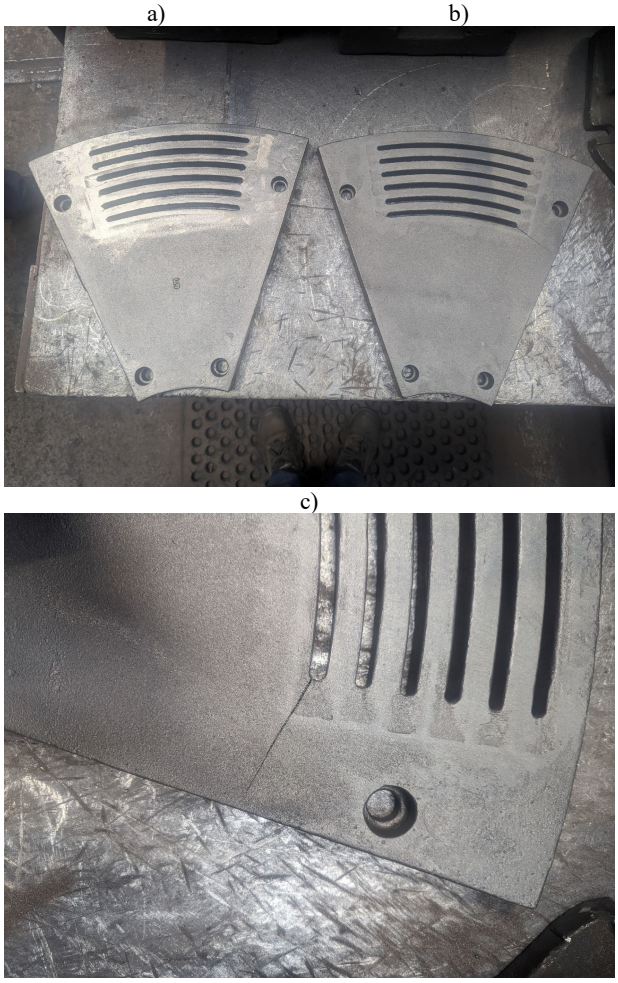

Fig. 22. Examples of chromium cast iron retaining wall castings: a) Fe-Nb inoculated cast iron casting without cracks; b) uninoculated cast iron casting with cracks; c) close-up of the crack area;

6. Conclusions

1. Under industrial conditions at the "Swidnica" Foundry Ltd, using the Althoff-Radtke test, it was shown that inoculating Fe-Ti and Fe-Nb eliminates defects in chromium cast iron produced from low-cost feedstock materials. However, observations made directly in industry show that Fe-Nb gives more consistent results in preventing porosity and hot cracks.
2. The Althoff-Radtke test has been successfully adopted in industrial conditions as a method for rapid assessment of the quality of high-chromium cast iron alloys.
3. The use of Fe-Nb as a inoculant allows for the production of castings from high-quality chromium cast iron that is resistant to hot cracking and free from internal defects, with repeatable impact values.
4. The inoculation allows optimum performance properties to be obtained for castings made of iron produced from low-quality metal raw material. Optimal properties are understood to be, for example, reproducible impact strength values and increased hardness in castings with lower carbon content and inoculated Fe-Nb
5. Hardening at a temperature of 950ºC allows the relevant properties of the castings to be obtained
6. The use of small amounts of Fe-Ti and Fe-Nb inoculants has a different effect on the microstructure of cast iron. In the first case, TiC carbides are formed first, resulting in the fragmentation of the primary austenite. In the case of the second inoculant, niobium strengthens the metal matrix and influences the crystallization of the residual liquid, forming niobium carbides.

References

[1] Kolokoltsev, V., Konopka, Z., Petrochenko, E. (2013). *Special cast iron. Types, casting, heat treatment, properties*. Częstochowa: Politechniak Częstochowska. (in Polish).

[2] Ngqase, M. & Pan, X. (2020). An overview on types of white cast irons and high chromium white cast irons. *Journal of Physics: Conference Series*. 1495, 012023. DOI: 10.1088/1742-6596/1495/1/012023.

[3] Purba, R.H., Shimizu, K., Kusumoto, K., Todaka, T., Shirai, M., Hara, H. & Ito, J. (2021). Erosive wear characteristics of high-chromium based multi-component white cast irons. *Tribology International*. 159, 106982, 1-9. https://doi.org/10.1016/j.triboint.2021.106982.

[4] DeMello, J.D.B., Durand-Charre, M. & Hamar-Thibault, S. (1983). Solidification and solid state transformations during cooling of chromium-molybdenum white cast irons. *Metallurgical Transactions A*. 14(9), 1793-1801. https://doi.org/10.1007/BF02645549.

[5] Studnicki, A., Kilarski, J., Przybył, M., Suchoń, J. & Bartocha, D. (2006). Wear resistance of chromium cast iron–research and application. *Journal of Achievements in Materials and Manufacturing Engineering*, 16(1-2), 63-73.

[6] Studnicki A., Dojka, R., Gromczyk, M. & Kondracki, M. (2016). Influence of titanium on crystallization and wear resistance of high chromium cast iron. *Archives of Foundry Engineering*. 16(1), 17-23. DOI: 10.1515/afe-2016-0014.

[7] Tian, H.H., Addie, G.R. & Pagalthivarthi, K.V. (2005). Determination of wear coefficients for erosive wear prediction through Coriolis wear testing. *Wear*. 259(1-6), 160-170. https://doi.org/10.1016/j.wear.2005.02.097.

[8] Tabrett, C.P., Sare, I.R. & Ghomashchi, M.R. (1996). Microstructure-property relationships in high chromium white iron alloys. *International Materials Reviews.* 41(2), 59-82. https://doi.org/10.1179/imr.1996.41.2.59.

[9] Kopyciński, D. (2015*). Shaping the structure and mechanical properties of cast iron intended for use in difficult conditions (selected issues)*. Katowice-Gliwice: Archives of Foundry Engineerung. (in Polish).

[10] Sobczak, J. (2013). *Foundryman's Handbook, Vol. 1, Contemporary Foundry.* Kraków: Wydawnictwo

Stowarzyszenia Technicznego Odlewników Polskich. (in Polish).
[11] Goto, I., Fukuchi, K. & Kurosawa, K. (2023). Effects of solidification conditions on the microstructural morphologies and strengths of hypereutectic high-chromium white cast iron castings. *Materials Science and Engineering: A.* 886, 145692, 1-15. https://doi.org/10.1016/j.msea.2023.145692.
[12] Bedolla-Jacuinde, A., Guerra, F.V., Guerrero-Pastran, A.J., Sierra-Cetina, M.A. & Valdez-Medina S. (2021). Microstructural effect and wear performance of high chromium white cast iron modified with high boron contents. *Wear*. 476, 203675, 1-10. https://doi.org/10.1016/j.wear.2021.203675.
[13] Barutçuoğlu, B., Koç, F. G., Erişir, E. & Karaarslan, G. (2025). The effect of tempering temperature on microstructure and wear behavior of tungsten and boron alloyed Ni-Hard 4 white cast irons. *International Journal of Metalcasting.* 19(1), 480-495. https://doi.org/10.1007/s40962-024-01322-8.
[14] Zou, W. Q., Zhang, Z. G., Yang, H. & Li, W. (2016). Effect of vibration frequency on microstructure and performance of high chromium cast iron prepared by lost foam casting. *China Foundry.* 13(4), 248-255. https://doi.org/10.1007/s41230-016-6037-3.
[15] Sakwa, W., Jura, S., Sakwa, J. (1980). *Abrasion-resistant iron alloys. Part I. Cast Iron*. Kraków: Wydawnictwo ZG STOP. (in Polish).
[16] Maratray, F., Usseglio-Nanot, R. (1971). Atlas - transformation characteristics of chromium and chromium-molybdenum white irons. Paris, France: Climax Molybdenum. 230.
[17] Huang, X. & Wu, Y. (1998). A high Cr-Mo alloy iron. *Journal of materials engineering and performance*. 7(4), 463-466. https://doi.org/10.1361/105994998770347594.
[18] Zumelzu, E., Cabezas, C., Opitz, O., Quiroz, E., Goyos, L. & Parada, A. (2003). Microstructural characteristics and corrosion behaviour of high-chromium cast iron alloys in sugar media. *Protection of Metals*. 39,183-188.
[19] Studnicki, A. (2008). Effect of boron carbide on primary crystallization of chromium cast iron. *Archives of Foundry Engineering*. 8(1), 173-176. ISSN (1897-3310).
[20] Yaer, X., Shimizu, K., Matsumoto, H., Kitsudo, T., Momono, T. (2008). Erosive wear characteristics of spheroidal carbides cast iron. *Wear*. 264(11-12), 947-957. https://doi.org/10.1016/j.wear.2007.07.002.
[21] Bedolla-Jacuinde, A., Hernández, B. & Béjar-Gómez, L. (2005). SEM study on the M7C3 carbide nucleation during eutectic solidification of high chromium white irons. *International Journal of Materials Research*. 96(12), 1380-1385.
[22] Bedolla-Jacuinde, A. & Rainforth, W.M. (2001). The wear behaviour of highchromium white cast irons as a function of silicon and mischmetal content. *Wear*. 250(1-12), 449-461. https://doi.org/10.1016/S0043-1648(01)00633-0.
[23] Bedolla-Jacuinde, A. (2001). Microstructure of vanadium-, niobium- and titanium-alloyed high-chromium white cast irons. *International Journal of Cast Metals Research*. 13(6), 343-361. https://doi.org/10.1080/13640461.2001.11819416.
[24] Carpentera, S.D., Carpenterb, D. & Pearcec, J.T.H. (2004). XRD and electron microscope study of an as-cast 26.6% chromium white iron microstructure. *Materials Chemistry and Physics*. 85(1), 32-40. https://doi.org/10.1016/j.matchemphys.2003.11.037.
[25] Laird, G., Nielsen, R.L. & Macmillan, N.H. (1991). On the nature of eutectic carbides in Cr-Ni white cast irons. *Metallurgical Transactions A*. 22A, 1709-1719. https://doi.org/10.1007/BF02646494.
[26] Chung, R.J. (2014). *Comprehensive study of the abrasive wear and slurry erosion behavior of an expanded system of high chromium cast iron and microstructural modification for enhanced wear resistance.* University of Alberta, Canada.
[27] Srivastava, A.K. & Das, K. (2009). Microstructural and Mechanical Characterization of in situ TiC and (Ti,W)C-reinforced high manganese austenitic steel matrix composites. *Materials Science and Engineering: A.* 516(1-2), 1-6. https://doi.org/10.1016/j.msea.2009.04.041.
[28] Das, K., Bandyopadhyay, T.K., & Das, S. (2001). A review on the various synthesis routes of TiC reinforced ferrous based composites. *Journal of materials science.* 37(18), 3881-3892. https://doi.org/10.1023/A:1019699205003.
[29] Olejnik, E., Janas, A., Kolbus, A. & Sikora, G. (2011). The composition of reaction substrates for TiC carbides synthesis and its influence on the thickness of iron casting composite layer. *Archives of Foundry Engineering.* 11(2), 165-168. ISSN (1897-3310).
[30] Olejnik, E., Tokarski, T., Sikora, G., Sobula, S., Maziarz, W., Szymański, Ł. & Grabowska, B. (2019). The effect of Fe addition on fragmentation phenomena, macrostructure, microstructure, and hardness of TiC-Fe local reinforcements fabricated in situ in steel casting. *Metallurgical and Materials Transactions A.* 50(2), 975-986. https://doi.org/10.1007/s11661-018-4992-6.
[31] Sobula, S., Olejnik, E. & Tokarski, T. (2017). Wear resistance of tic reinforced cast steel matrix composite. *Archives of Foundry Engineering.* 17(1), 143-146. ISSN (1897-3310).
[32] Szymański, Ł., Olejnik, E., Tokarski, T., Kurtyka, P., Drożyński, D. & Żymankowska-Kumon, S. (2018). Reactive casting coatings for obtaining in situ composite layers based on Fe alloys. *Surface and Coatings Technology*. 350, 346-358. https://doi.org/10.1016/j.surfcoat.2018.06.085.
[33] Szymański, Ł., Olejnik, E., Sobczak, J.J., Szala, M., Kurtyka, P., Tokarski, T. & Janas, A. (2022). Dry sliding, slurry abrasion and cavitation erosion of composite layers reinforced by TiC fabricated in situ in cast steel and gray cast iron. *Journal of Materials Processing Technology*. 308, 117688, 1-15. https://doi.org/10.1016/j.jmatprotec.2022.117688.
[34] Głownia, J., Tęcza, G., Asłanowicz, M. & Ościłowski, A. (2013). Tools cast from the steel of composite structure. *Archives of Metallurgy and Materials*. 58(3), 803-808. DOI: 10.2478/amm-2013-0075.
[35] Kalandyk, B., Tęcza, G., Zapała, R., & Sobula, S. (2015). Cast high-manganese steel - the effect of microstructure on abrasive wear behaviour in Miller test. *Archives of Foundry Engineering.* 15(2), 35-38. DOI: 10.1515/afe-2015-0033.

[36] Tęcza, G. & Głownia, J. (2015). Resistance to abrasive wear and volume fraction of carbides in cast high-manganese austenitic steel with composite structure. *Archives of Foundry Engineering.* 15(4), 129-133. DOI: 10.1515/afe-2015-0092.
[37] Tęcza, G. & Garbacz-Klempka, A. (2016). Microstructure of cast high-manganese steel containing titanium. *Archives of Foundry Engineering.* 16(4), 163-168. ISSN (1897-3310).
[38] Tęcza, G. & Zapała, R. (2018). Changes in impact strength and abrasive wear resistance of cast high manganese steel due to the formation of primary titanium carbides. *Archives of Foundry Engineering.* 18(1), 119-122. DOI: 10.24425/118823.
[39] Tęcza, G. (2021). Changes in abrasive wear resistance during Miller test of high-manganese cast steel with niobium carbides formed in the alloy matrix. *Applied Sciences.* 11(11), 4794, 1-10. https://doi.org/10.3390/app11114794.
[40] Tęcza, G. (2021). Changes in abrasive wear resistance during miller test of Cr-Ni cast steel with Ti carbides formed in the alloy matrix. *Archives of Foundry Engineering.* 21(1), 110-115. DOI: 10.24425/afe.2021.139758.
[41] Tęcza, G. (2022). Changes Changes in microstructure and abrasion resistance during Miller test of Hadfield high-manganese cast steel after the formation of vanadium carbides in alloy matrix. *Materials*. 15(3), 1021, 1-11. https://doi.org/10.3390/ma15031021.
[42] Tęcza, G. (2023). Changes in abrasion resistance of cast Cr-Ni steel as a result of the formation of niobium carbides in alloy matrix. *Materials*. 16(4), 1726, 1-14. https://doi.org/10.3390/ma16041726.
[43] Tęcza, G. (2023). Changes in the microstructure and abrasion resistance of tool cast steel after the formation of titanium carbides in the alloy matrix. *Archives of Foundry Engineering*. 23(4), 173-180. DOI: 10.24425/afe.2023.148961.
[44] Studnicki, A., & Szajnar, J. (2012). Testing the wear resistance of low-alloy and chromium cast steel. *Archives of Foundry Engineering*. 12(2), 79-84. ISSN (1897-3310).
[45] Studnicki, A., Kondracki, M., Suchoń, J., Szajnar, J., Bartocha, D. & Wróbel, T. (2015). Abrasive wear of alloyed cast steels applied for heavy machinery. *Archives of Foundry Engineering*. 15(1), 99-104. ISSN (1897-3310).
[46] Cuppari, M.G.D.V. & Santos, S.F. (2016). Physical properties of the NbC carbide. *Metals*. 6(10), 250, 1-17. https://doi.org/10.3390/met6100250.
[47] Ross R.B. (1992). *Metallic Materials Specification Handbook*, 4th edn,. London: Chapman and Hall.
[48] Studnicki, A. (2002). Investigation of crystallization process of wear resistant cast iron. *Archives of Foundry.* 2(4), 259-264. ISSN (1642-5308). (in Polish).
[49] Bedolla-Jacuinde, A. (2016). Niobium in cast irons. In V.Glebovsky (Eds.), *Progress in Metallic Alloys* (pp. 187-220). Croatia: InTech. http://dx.doi.org/10.5772/64498.
[50] Mohrbacher, H., Jarreta, D. (2015). Technology, Properties and Applications of NbC Reinforced Steel and Iron Alloys, In Proceedings of the Symposium on Fundamentals and Applications of Mo and Nb Alloying in High Performance Steels.
[51] Guesserm W.L. (1985). Using niobium in high-chromium irons. *Foundry Management Technology*.
[52] Zhou, Y., Yang, Y., Yang, J., Hao, F., Li, D., Ren, X. & Yang, Q. (2021). Effect of Ti additive on (Cr, Fe)7C3 carbide in arc surfacing layer and its refined mechanism, *Applied Surface Science*. 258(17), 6653-6659. https://doi.org/10.1016/j.apsusc.2012.03.101.
[53] Zhang, Y.C., Song, R.B., Yu, P., Wen, E. & Zhao, Z.Y. (2020). The formation of TiCeNbC coreshell structure in hypereutectic high chromium cast iron leads to significant refinement of primary M7C3. *Journal of Alloys and Compounds*. 824, 153806, 1-10. https://doi.org/10.1016/j.jallcom.2020.153806.
[54] Qu, Y., Xing, J., Zhi, X., Peng, J. & Fu, H. (2008). Effect of cerium on the as-cast microstructure of a hypereutectic high chromium cast iron. *Materials Letters.* 62(17-18), 3024-3027. https://doi.org/10.1016/j.matlet.2008.01.129.
[55] Wu, X.J., Xing, J.D., Fu, H.G. & Zhi, X.H. (2007). Effect of titanium on the morphology of primary M7C3 carbides in hypereutectic high chromium white iron. *Materials Science and Engineering: A.* 457(1-2), 180-185. https://doi.org/10.1016/j.msea.2006.12.006.